Available online at www.sciencedirect.com
ScienceDirect
Trans. Nonferrous Met. Soc. China 32(2022) 3801−3809
Transactions of Nonferrous Metals Society of China
www.tnmsc.cn

One-step production of high-strength titanium alloy by sintering titanium hydride powder from upgraded titania slag

Zhao-wang DONG[1,2], Yang XIA[1], Xue-yi GUO[1,2], Qing-hua TIAN[1,2], Han-ning LIU[1,2], Pei-dong LIU[1], Yu-bing CHEN[1]

1. School of Metallurgy and Environment, Central South University, Changsha 410083, China;
2. Research Institute of Resource Recycling, Central South University, Changsha 410083, China

Received 23 August 2021; accepted 28 February 2022

Abstract: A direct production method of high-strength titanium alloy from upgraded titania slag (UGS) was developed. First, UGS was reduced into alloy powder with 1.3 wt.% oxygen using magnesium powder. Subsequently, the alloy powder was compacted at 600 MPa to produce a pellet. Lastly, the pellet was sintered to produce titanium alloy. The reduced powder was characterized, and the effect arising from the sintering temperature on the sintered density, compressive strength, microstructure, and hardness of the alloys was studied. The results showed that the density tended to increase with the temperature increasing from 900 to 1200 °C, whereas the porosity decreased. A significant sintering densification was achieved at the temperature above 1100 °C (98.65% at 1100 °C and 99.41% at 1200 °C). At 1100 °C, the hardness and compressive strength reached the maximal values of the alloy, HV 655.7 and 1563 MPa, respectively.
Key words: upgraded titania slag; reduction; titanium alloy; sintering

1 Introduction

Titanium alloys are of instrumental significance because of favorable properties (e.g., enhanced resistance to corrosion, high strength performance, low density, as well as high-temperature durability). Thus, they have been applied in extensive industrial fields from aerospace to sporting goods [1−4]. Most titanium products are derived from upgraded titania slag (UGS) through the Kroll process, followed by casting and thermomechanical processing [5]. Since titanium exhibits poor machinability, the buy-to-fly ratio is generally high (>5:1), thus causing high production costs. Powder metallurgy, a near-net-shape technique, can potentially act as a more economical production method for titanium alloys for its high material utilization [6]. The existing processes for producing Ti-based alloy (the FFC process [7], the Armstrong process [8], the TiRO process [9], and the CSIR process [10]) via powder metallurgy have employed either $TiCl_4$ or pure TiO_2 as precursors. $TiCl_4$ and TiO_2 are synthesized using UGS through the chloride processes, both of which are reported to be energy-intensive and environmentally damaging.

As demonstrated by our recent study [11], the titanium hydride powder can be synthesized by a one-step Mg reduction, which achieves an oxygen level of ~1 wt.%. Oxygen atoms are capable of increasing the degree of distortion in the metal crystal lattice, the internal strain capacity and the dislocation motion resistance, while improving the strength and hardness of the alloy [12]. CHEN et al [13] added oxygen into the Ti lattice using two different powder metallurgy methods, which proved that a high elongation at break of higher than 20% could be achieved from samples with a yield pressure over 800 MPa.

Corresponding author: Yang XIA, Tel: +86-731-88877863, E-mail: yang.xia@csu.edu.cn;
Xue-yi GUO, Tel: +86-731-88879201, E-mail: xyguo@csu.edu.cn
DOI: 10.1016/S1003-6326(22)66059-X

In this work, UGS was reduced with Mg powder under hydrogen flow. Titanium hydride powder was produced, of which the oxygen content was kept to a mass fraction of 1.3% and a particle size of <16 μm. The powder was compacted at 600 MPa to produce a pellet to conduct the sintering densification study. The sintering temperature was found to have some effects on the microstructure, sintered density, compressive strength and hardness of the sintered sample, which were investigated specifically. The preparation method of titanium alloy powder by sintering titanium powder produced through magnesium thermal reduction of UGS was proved theoretically and experimentally to be feasible, which could be used as a shorter production route for the comprehensive utilization of UGS.

2 Experimental

UGS, the raw material, was provided by Rio Tinto. The flux and anhydrous reducing agent were $MgCl_2$ powder (Shanghai Aladdin Bio-Chem Technology Co., Ltd.) and Mg powder with particle size of 74−100 μm (Sinopharm Chemical Reagent Co., Ltd.), respectively. Figure 1 illustrates the main process of the experiment.

The UGS was first processed by a mill into powder and this powder was sifted with a grid mesh to precisely adjust the particle size at 38 μm. Subsequently, those fine powders of UGS, anhydrous $MgCl_2$ and Mg were added at a specific mass ratio 1:1.5:0.2 to mix for 15 min, the mixture above was placed in a Mo crucible, and the mixture was reduced in a tube furnace (TF14P80 TAISITE). Next, the H_2 flow for the mixture reduction was maintained with 1 L/min at approximately 750 °C for 4 h. After the reduction, the product was cooled to 30 °C, followed by the addition of deionized (DI) water to produce a slurry. Afterward, CH_3COOH was slowly added into the slurry to adjust the pH from 3 to 5. After the resulting sample was leached in acetic acid, the insoluble powder was purified with DI water and C_2H_5OH. Then, the powder was dried at 50 °C for 12 h. The reduced powder product was compacted at a tablet pressure of 600 MPa to produce a pellet (with a diameter of 10 mm and a height of 12 mm). Furthermore, the pellet was loaded into a corundum crucible. Under an Ar atmosphere, it was heated to a temperature ranging from 900 to 1200 °C in a tube furnace and kept for 2 h. Lastly, the alloy product was cooled till its temperature was close to ambient temperature, and the sintered products were exploited for mechanical property tests.

The raw materials and the product at the respective step were characterized using back titration based on ethylene diamine tetraacetic acid (EDTA), scanning electron microscopy (SEM) with energy dispersive spectroscopy (EDS), as well as X-ray diffraction (XRD) based on a PANalytical X'Pert X-ray diffractometer (Cu K_α radiation) and a D8 Discover 2500 analyzer. An oxygen and nitrogen analyzer (LECO TCH−600) was adopted to analyze the oxygen content of the obtained powder product. A laser particle size analyzer (Mastersizer 2000) was adopted to examine the particle size distribution of the reduced powder, and Brunauer–Emmett–Teller (BET) surface area analysis (JW-BK222) was conducted to determine the specific surface area of the reduced powder. Using the Archimedes method, the densities of the sintered alloys were measured. The pore-filling liquid was Mobil DI.TE25 oil, and the test liquid was a hydrofluoroplyether heat transfer fluid. The theoretical density (ρ_{th}, TD) was calculated by [14]

$$\rho_{th} = 100/(\frac{m_{Ti}}{\rho_{Ti}}+\frac{m_{Fe}}{\rho_{Fe}}+\frac{m_{Al}}{\rho_{Al}}+\frac{m_{Si}}{\rho_{Si}}+\frac{m_{Cr}}{\rho_{Cr}}+\frac{m_{Mn}}{\rho_{Mn}}) \quad (1)$$

where m_i and ρ_i (i=Ti, Fe, Al, Si, Cr, Mn) denote the mass fraction and density of constituent i, respectively. The TD of the alloy applied in this work, calculated by Eq. (1), was 4.677 g/cm^3.

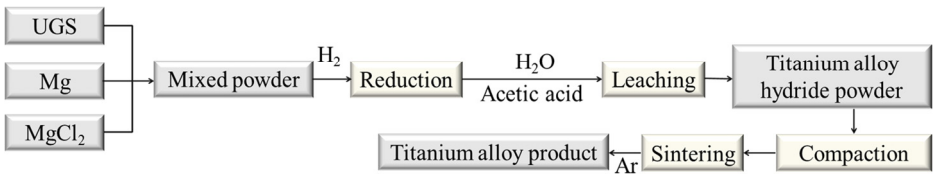

Fig. 1 Flow chart of reduction of UGS and sintering of powder reduced from UGS to prepare Ti alloy

The sintering behavior of the product was measured with a dilatometer (coefficient of thermal expansion tester-PCY series). The hardness and compression properties of the sintered alloy were measured with a Vickers hardness tester (HVS−50) and an electronic universal material testing machine (Instron 5969), respectively. To gain more insights into the sintering behavior, phase and microstructure evolution, thermodynamic modeling was built using the commercial Pandat software under the titanium database.

3 Results and discussion

3.1 Reduced powder

3.1.1 Powder composition and evolution of minor elements

To study the exact chemical composition of the untreated material of UGS, a back titration with EDTA was proceeded with the Leco combustion analyzer, and the results are listed in Table 1.

Table 1 Element compositions of UGS and reduced powder (wt.%)

Sample	Ti	Fe	Si	Al	Cr	Mn	O
UGS	54.86	2.68	0.93	0.18	0.47	0.34	39.72
Reduced powder	90.85	3.87	1.05	0.53	0.61	0.46	1.30

Ti, Fe, Si, Al, Cr, Mn and O in the UGS had the compositions of 54.86, 2.68, 0.93, 0.18, 0.47, 0.34, and 39.72 wt.%, respectively. In addition, several minor metal elements (e.g., 0.06 wt.% Cu, 0.07 wt.% Ni, and 0.08 wt.% Mg) were detected. The hydrogen content of the reduced powder was measured as 3.87 wt.%. The compositions of all metals in the powder product were improved after the reduction in H_2 atmosphere, whereas those of oxygen decreased significantly, indicating the successful reduction of metal elements. The minimal oxygen content of ~2.5 wt.% was measured during Mg reduction of TiO_2 in an Ar atmosphere. As previously demonstrated by thermodynamic modeling, the Mg deoxidation limit of TiO_2 in an Ar atmosphere at 750 °C was higher than 2 wt.% [15−17]. In this work, a 1.3 wt.% oxygen content was obtained, significantly lower than the theoretical deoxidation limit of Mg. The above result was achieved possibly due to the use of hydrogen, which was found to decrease the Ti−O solid solution stability and subsequently facilitate the deoxidation process. To evaluate the possibility of the deoxygenation of Ti by Mg in H_2, the oxygen potential in TiH_yO_x synthesized by Reaction (2) was compared with that in MgO synthesized by Reaction (3) and TiO_x synthesized by Reaction (4). Oxygen potentials at 700 °C in MgO, TiO_x, and TiH_yO_x with 2 wt.% oxygen were determined according to Refs. [18,19], and the results are presented in Fig. 2.

$$Ti+y/2H_2+x/2O_2\rightarrow TiH_yO_x \quad (2)$$

$$2Mg+O_2\rightarrow 2MgO \quad (3)$$

$$Ti+x/2O_2\rightarrow TiO_x \quad (4)$$

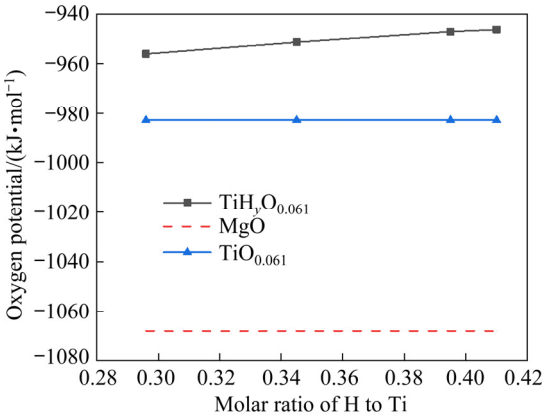

Fig. 2 Comparison of oxygen potential in MgO, $TiH_yO_{0.061}$, and $TiO_{0.061}$

It was assumed that the Ti−O solid solution contained 2 wt.% oxygen, i.e., x=0.061, and y denotes the molar ratio of H to Ti. According to Fig. 2, the oxygen potential in TiH_yO_x was less than that in TiO_x, thus indicating that hydrogen destabilized Ti−O solid solutions, which increased the driving force for Mg to capture oxygen from Ti−O solutions. Accordingly, a one-step Mg reduction in a hydrogen atmosphere could yield a titanium product with significantly lower oxygen content.

3.1.2 Morphology, particle size distribution, and phase composition

Figures 3(a) and (b) present the morphologies of the untreated material and the reaction product, respectively. The elementary composition of the product powder was analyzed through EDS mapping (Figs. 3(c–j)).

The distribution of metal elements, instead of Ti and Al, was relatively inhomogeneous. Fe and Si were segregated in several areas. Figure 4 clearly

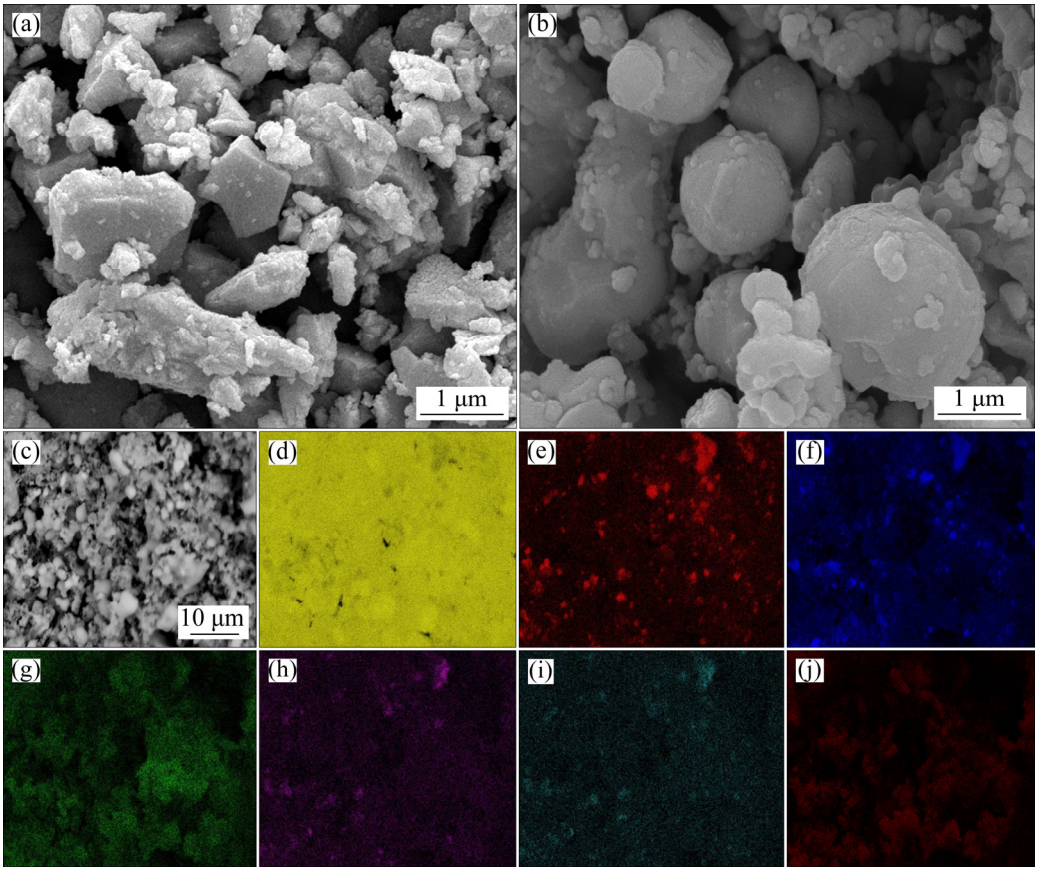

Fig. 3 SEM images of morphology of UGS raw material (a) and reduced powder (b), backscattered electron image of reduced powder (c), and EDS maps of Ti (d), Fe (e), Si (f), Al (g), Cr (h), Mn (i) and O (j)

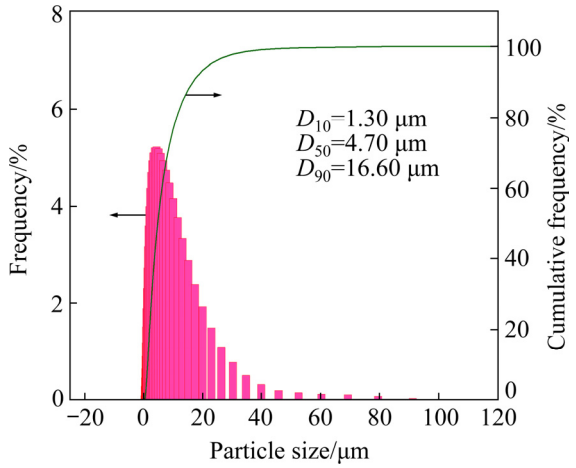

Fig. 4 Particle size distribution of reduced powder

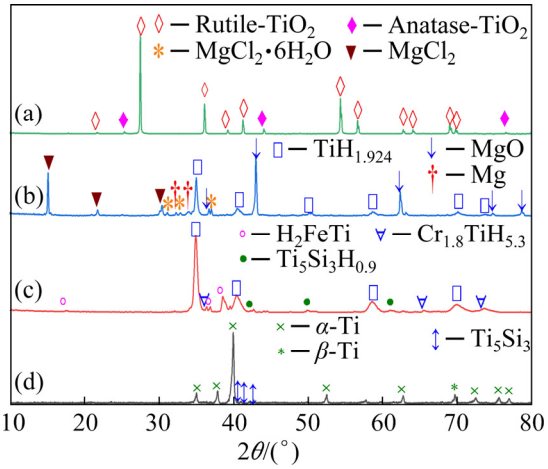

Fig. 5 XRD patterns of raw material and product at respective step: (a) Raw material; (b) Reduced and unleached powder; (c) Reduced and leached powder; (d) Sintered alloy

presents the particle size distribution. D_{10}, D_{50} and D_{90} of the reduced powder reached 1.30, 4.70 and 16.60 μm, respectively.

The results of XRD analysis are shown in Fig. 5. To clarify the phase changes before and after reduction at the respective step, the analysis of XRD was conducted for the powder product at every reaction stage.

The major TiO_2 phase of the raw material was rutile phase, while the other less proportion of the TiO_2 was anatase phase. Through titration with EDTA, SiO_2, Al_2O_3 and other metal oxides were detected. The above components were limited, and

it would be difficult to detect through conventional XRD analysis. After the reduction but before the leaching process, $MgCl_2$, TiH_2 and MgO were identified in the products. Furthermore, superfluous Mg and a small amount of $MgCl_2{\cdot}6H_2O$ were identified. The phases of $Cr_{1.8}TiH_{5.3}$, HFe_2Ti, and $Ti_5Si_3H_{0.9}$ in the reduced powder might represent the bright phases observed in the EDS mapping images (Fig. 3).

3.2 Sintered alloys

As revealed by the XRD pattern of the as-sintered alloy (Fig. 5), only Ti_5Si_3 was identified besides α-Ti and β-Ti. Cr and Fe were beta stabilizers. After sintering at a high temperature (>900 °C), Ti_5Si_3 was found with the potential to dissolve into Ti, which could explain why $Cr_{1.8}TiH_{5.3}$ and HFe_2Ti were not detected. Furthermore, dehydrogenation occurred at a high temperature, thus leading to the formation of α-Ti, β-Ti and Ti_5Si_3.

The densities of the sintered alloys increased with the increase in the sintering temperature (Fig. 6). At 900 °C, the density was approximately 90% (TD). At the temperatures above 1100 °C, an increasing sintered density (98.65% TD at 1100 °C, and 99.41% TD at 1200 °C) was achieved.

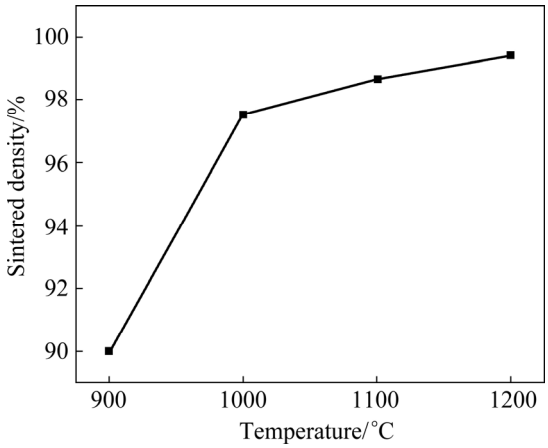

Fig. 6 Densities of sintered alloys at different temperatures

Figure 7 presents the microstructures of the sintered alloys formed at different sintering temperatures. A significant drop in porosity was correlated with the gradual increase in the sintering temperature. At 900 °C, the cross-section of the sample showed a certain number of pores with a size <5 μm. The pores were primarily concentrated in the gray titanium-rich area, probably arising from the dehydrogenation of titanium hydride during sintering, which affected the porosity of the reduced powder compacts. The three possible factors of the

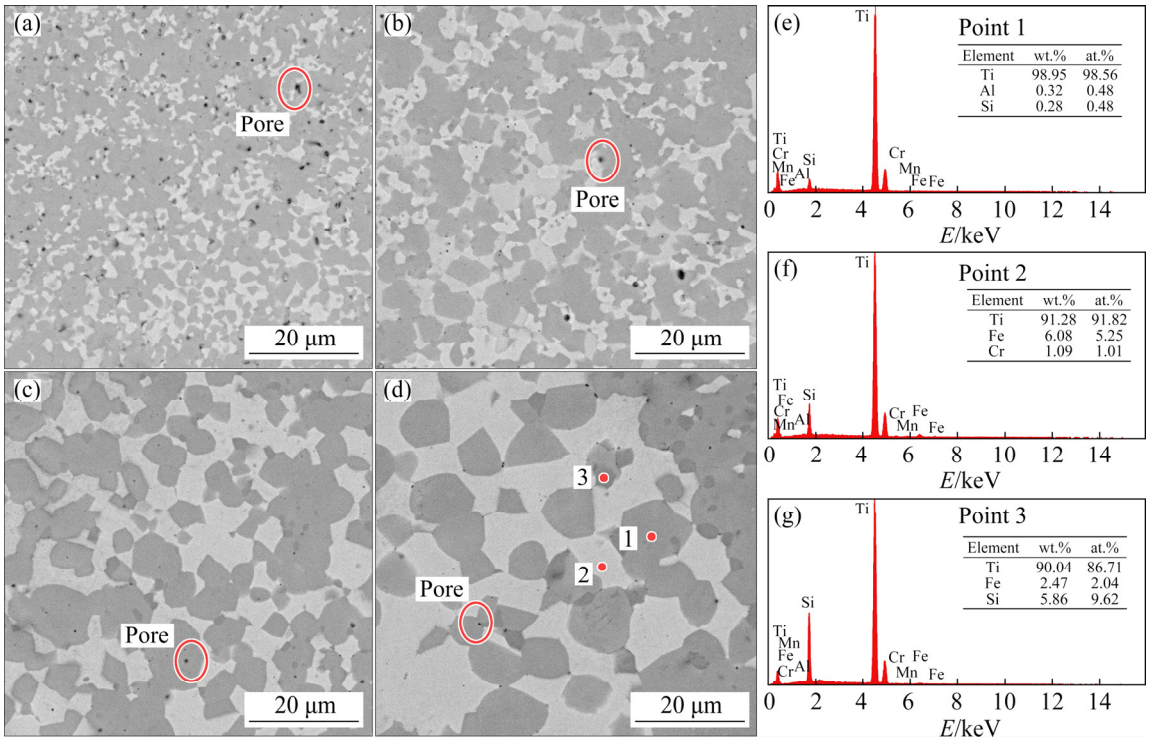

Fig. 7 SEM images of sintered product at 900 °C (a), 1000 °C (b), 1100 °C (c) and 1200 °C (d), and corresponding EDS results of Point 1 (e), Point 2 (f) and Point 3 (g)

pore formation are elucidated below: (1) The shrinking original powder particles and instantaneous dehydrogenation increased the inter-particle spacing; (2) The released gas might take up the place of the originally close-packed particles. At the early stages of dehydrogenation and pre-sintering, the main process was the pulverization of the hydride particles and inter-particle separation [20,21]; (3) The reduced powder was not pure titanium hydride and might also contain other elements, thus probably leading to a certain resistance to the process of hydrogen diffusion. Accordingly, the driving force for the diffusion of hydrogen and other elements would be insufficient at low sintering temperatures. The inadequate diffusion led to the retention of the pores in the alloy in the sintered products at 900 °C. It can be seen from Fig. 7 that, a number of pores emerge significantly and decrease at 1000 and 1100 °C. At 1200 °C, nearly full densification was achieved. As revealed by EDS point analysis, three phase regions, including the gray phase region (Point 1), bright phase region (Point 2) and dark phase region (Point 3), might represent the phases of α-Ti, β-Ti and Ti_5Si_3, respectively.

EDS mapping of the alloy obtained at 1200 °C (Fig. 8) clearly shows the distribution of different elements in the alloy. The beta stabilizers of Fe, Cr, and Mn were concentrated in the β-Ti phase region, while Si was concentrated in the dark phase region (Ti_5Si_3), and Al was homogenously distributed throughout the alloy.

To gain more insights into the formation of the phases and the microstructures of the alloys, CALPHAD software (Pandat) under the titanium alloy database was employed to simulate the phase composition of the alloy at the temperatures of 100−1500 °C (Fig. 9(a)).

Between 100 and 600 °C, the main equilibrium phases in the system included the HCP phase (namely α-Ti), Ti_5Si_3, and Laves-C_{14}. After the sintering process, the alloy was furnace-cooled to 30 °C, and considerable beta phases might not have been transferred, thus leading to a beta phase appearing in the final alloy. There might be two reasons for the formation of Ti_5Si_3 phase in the alloy. The first step was that a small amount of Ti_5Si_3 phase was generated during the reduction. The process of magnesium reduction of high titanium slag refers to a self-propagating reaction, which released considerable heat violently, thus leading to a rapid rise in the temperature of the reaction system, and the Ti_5Si_3 phase was generated from the reduced Ti and Si elements. Besides, due to the aggregation of Si, Ti_5Si_3 phase was formed during the sintering step. The Laves-C_{14} phase refers to the high melting point phase formed by Cr element in alloy with refractory metal element Nb. The model was consistent with the XRD and SEM results. Moreover, it is noteworthy that some liquid phases were formed above 1000 °C. Figure 9(b) presents the correlation between the liquid phase composition and temperature when the system was in either equilibrium or non-equilibrium state.

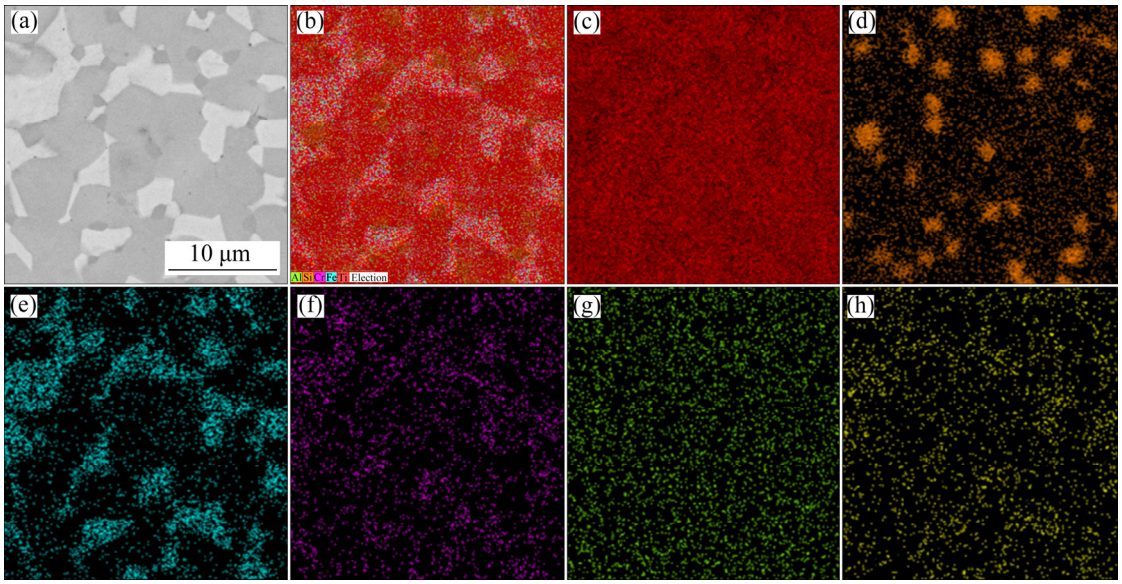

Fig. 8 SEM image (a), and combination (b) and individual (c−h) EDS mapping images of sintered product at 1200 °C: (c) Ti; (d) Fe; (e) Si; (f) Cr; (g) Al; (h) Mn

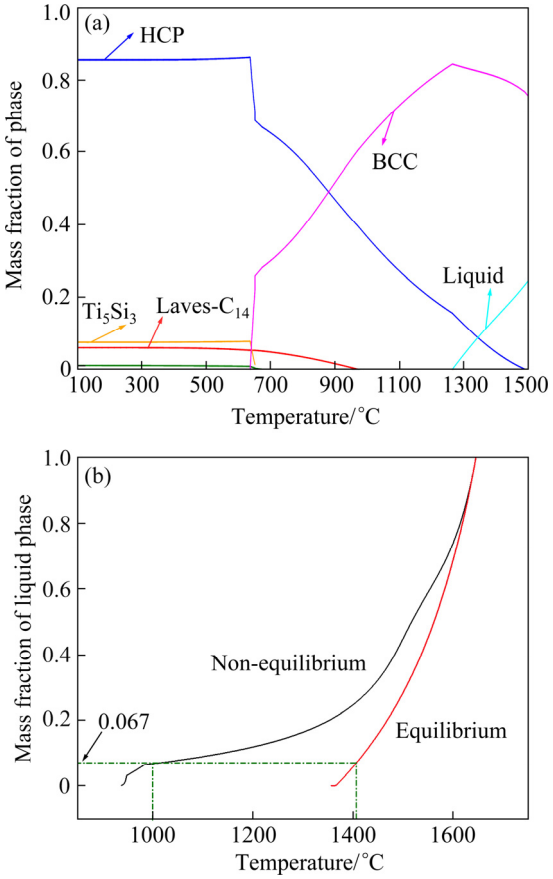

Fig. 9 Phase composition of alloy from 100 to 1500 °C (a), and relationship between liquid phase fraction and temperature (b)

Elements (e.g., Fe and Cr) were limited to the beta phase region, thus resulting in a non-equilibrium state. According to the non-equilibrium line, 6.7% liquid phase might be formed at around 1000 °C, and ~12% liquid phase might be formed at 1200 °C, thus leading to a liquid-surrounding environment during the sintering process.

3.3 Sintering behavior

Figure 10 plots the thermal expansion curve of the compacted pellet from 30 to 1200 °C in an Ar atmosphere.

Significant shrinkage was identified across two temperature ranges, including 425−690 °C and 908−1048 °C, respectively. The first temperature range fell within that of titanium dehydrogenation, which confirmed that most of titanium hydride in the sample was dehydrogenated before 700 °C, which is consistent with existing studies [22]. After hydrogen was released, the pellet shrunk under the significant difference in the densities of Ti and TiH_2. The second temperature range could represent

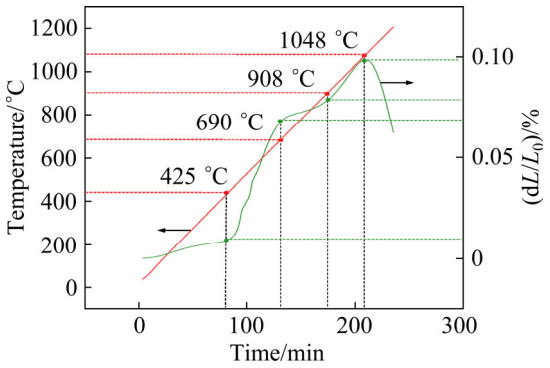

Fig. 10 Thermal expansion curve of compacted pellet from 30 to 1200 °C (dL/L_0 represents the shrinkage of alloy during heating)

the sintering of titanium powders. When the temperature ranged from 700 to 908 °C, the thermal expansion slowed down. This is possibly because the sintering temperature is too low to provide the driving force required for hydrogen release and sintering between particles. With the formation of Ti in the dehydrogenation reaction, some newly formed Ti particles may start to exhibit sintering necking. When the sintering process was carried out at a higher temperature of 1048 °C, the alloy shrank more, which revealed that the densification of the samples was more significantly intensified. The newly formed Ti particles were endowed with more activities, thus improving sintering necking of the above Ti particles, and facilitating densification. Interestingly, the sintered pellets started to expand at the temperatures higher than 1048 °C, probably arising from the appearing liquid phase in the reaction system. Thermodynamic modeling (Fig. 9(b)) revealed the exact existence of the liquid phase. When the system was heated to above 1048 °C, liquid-phase sintering would occur, thus leading to a better densification (Fig. 6).

3.4 Mechanical properties

Five points of the respective alloy section were selected to measure the Vickers hardness, and the mean value was determined (Fig. 11).

The Vickers hardness increased from HV 518.1 to HV 655.7 with the increase in the temperature from 900 to 1100 °C; however, when it was heated to 1200 °C, the Vickers hardness decreased to HV 646.8. The above result was probably because the resulting Vickers hardness was closely correlated with the internal structure of

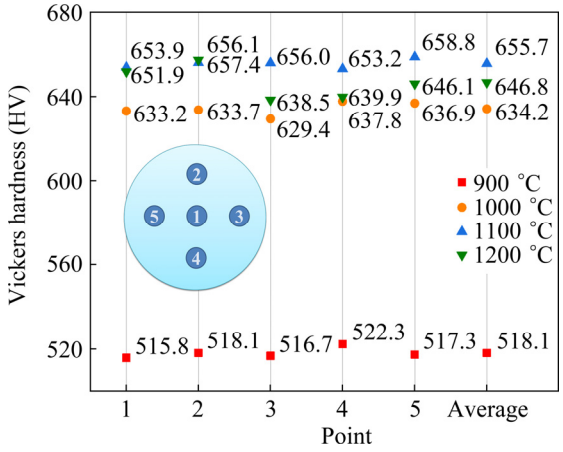

Fig. 11 Vickers hardness of sintered alloys at different temperatures

the sintered specimen after the completion of densification. After the specimen was heated to 1200 °C, the Vickers hardness decreased due to the subsequent grain coarsening.

The stress−strain compression curves of the sintered alloys at three temperatures are presented in Fig. 12. With the increase of the sintering temperature, the compressive strength of the sintered alloy increased at the beginning and then obvious decrease occurred after reaching the maximal value of 1563 MPa at 1100 °C. The reduction in the strength at 1200 °C could be attributed to the growth and coarsening of grains in the alloy.

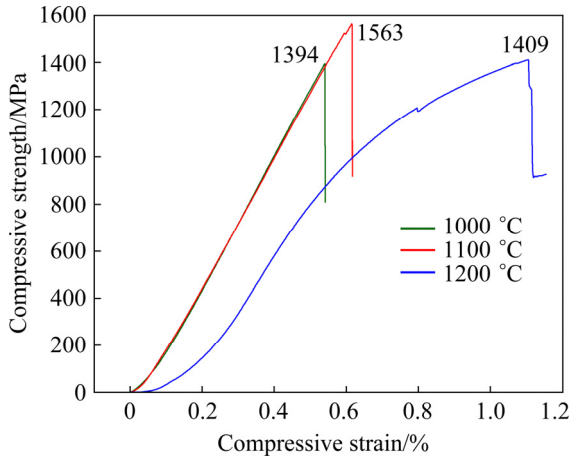

Fig. 12 Compressive strength of sintered alloy at different temperatures

4 Conclusions

(1) Titanium alloy hydride powder with 1.30 wt.% oxygen was well synthesized through a one-step reduction process from UGS. The powder composition was mainly formed by the $TiH_{1.924}$ phase (δ) and a small amount of intermetallic phases of H_2FeTi, $Ti_5Si_3H_{0.9}$ and $Cr_{1.8}TiH_{5.3}$.

(2) A significant sintering densification was achieved at the temperature above 1100 °C (98.65% TD at 1100 °C and 99.41% TD at 1200 °C). The hardness and compressive strength of the titanium alloy also reached maximal values of HV 655.7 and 1563 MPa, respectively, at 1100 °C.

(3) The existence of minor elements (e.g., Mn, Cr, and Fe) resulted in the formation of a liquid phase at a relatively low temperature (1000 °C), thus causing the sintering in a partially liquid state and leading to full densification. The synergistic reduction of metals in UGS and various elements on the properties of the alloy should be explored in depth.

Acknowledgments

This work was financially supported by the National Natural Science Foundation of China (No. 52004342), the Innovation-Driven Project of Central South University, China (No. 150240015), and the Natural Science Fund for Outstanding Young Scholar of Hunan Province, China (No. 2021JJ20065).

References

[1] LIU Yong, TANG Han-chun, HUANG Qian-li, ZHAO Da-peng, HE Jun-yang, CAO Yuan-kui, SONG Min, LIU Bin, OUYANG Si-hui. Strong-yet-ductile Ti−Zr alloys through high concentration of oxygen strengthening [J]. Transactions of Nonferrous Metals Society of China, 2020, 30(9): 2449−2458.

[2] XIA Yang, DONG Zhao-wang, GUO Xue-yi, TIAN Qing-hua, LIU Yong. Towards a circular metal additive manufacturing through recycling of materials: A mini review [J]. Journal of Central South University, 2020, 27(7): 1134−1145.

[3] LEI Ting. Titanium and titanium alloy [M]. Beijing: Metallurgical Industry Press, 2018. (in Chinese)

[4] GUO Xue-yi, DONG Zhao-wang, XIA Yang, LIU Pei-dong, LIU Han-ning, TIAN Qing-hua. Preparation low-oxygen-containing Ti−48Al−2Cr−2Nb alloy powder by direct reduction of oxides [J]. Transactions of Nonferrous Metals Society of China, 2022, 32: 1351−1361.

[5] WANG Tian, WANG Yao-wu, WANG Yu, HE Xiao-jun. Research progress of titanium metal smelting [J]. China Nonferrous Metallurgy, 2020 49(3): 1−6, 27. (in Chinese)

[6] FANG Z Z, PARAMORE J D, SUN P, CHANDRAN K S R, ZHANG Y, XIA Y, CAO F, KOOPMAN M, FREE M. Powder metallurgy of titanium–past, present, and future [J].

International Materials Reviews, 2018, 63(7): 407−459.
[7] LI Wei, WANG Ying, TANG Ren-heng, XIAO Fang-ming. Research development of preparation of titanium by the FFC Cambridge process [J]. Materials Research and Application, 2010, 4(4): 555−560. (in Chinese)
[8] CHEN W, YAMAMOTO Y, PETER W H, GORTI S B, SABAU A S, CLARK M B, NUNN S D, KIGGANS J O, BLUE C A, WILLIAMS J C, FULLER B, AKHTAR K. Cold compaction study of Armstrong process® Ti−6Al−4V powders [J]. Powder Technology, 2011, 214 (2): 194−199.
[9] DOBLIN C, FREEMAN D, RICHARDS M. The TiRO™ process for the continuous direct production of titanium powder [J]. Key Engineering Materials, 2013, 551: 37−43.
[10] van VUUREN D S, OOSTHUIZEN S J, SWANEPOEL J J. Development of a continuous process to produce Ti via metallothermic reduction of $TiCl_4$ in molten salt [J]. Key Engineering Materials, 2013, 551: 16−24.
[11] DONG Zhao-wang, XIA Yang, GUO Xue-yi, ZHAO Jin-long, JIANG Lin-feng, TIAN Qing-hua, LIU Yong. Direct reduction of upgraded titania slag by magnesium for making low-oxygen containing titanium alloy hydride powder [J]. Powder Technology, 2020, 368: 160−169.
[12] YU Q, QI L, TSURU T, TRAYLOR R, RUGG D, MORRIS J W Jr, ASTA M, CHRZAN D C, MINOR A M. Origin of dramatic oxygen solute strengthening effect in titanium [J]. Science, 2015, 347(6222): 635−639.
[13] CHEN Biao, SHEN Jiang-hua, YE Xiao-xin, UMEDA J, KONDOH K. Advanced mechanical properties of powder metallurgy commercially pure titanium with a high oxygen concentration [J]. Journal of Materials Research, 2017, 32(19): 3769−3776.
[14] XIA Y, LUO S D, WU X, SCHAFFER G B, QIAN M. The sintering densification, microstructure and mechanical properties of gamma Ti−48Al−2Cr−2Nb alloy with a small addition of copper [J]. Materials Science and Engineering A, 2013, 559: 293–300.
[15] XIA Yang, FANG Z, ZHANG Ying, LEFLER H, ZHANG Tuo-yang, SUN Pei, HUANG Zhe. Hydrogen assisted magnesiothermic reduction (HAMR) of commercial TiO_2 to produce titanium powder with controlled morphology and particle size [J]. Materials Transactions, 2017, 58(3): 355−360.
[16] FANG Z Z, SUN Pei. Pathways to optimize performance/cost ratio of powder metallurgy titanium—A perspective [J]. Key Engineering Materials, 2012, 520: 15−23.
[17] GUO Xue-yi, DONG Zhao-wang, XIA Yang, TIAN Qing-hua, ZENG Guang, ZHENG Ze-bang. Direct preparation of titanium alloy powder from upgraded titanium slag by magnesium reduction [J]. Chinese Journal of Rare Metals, 2021, 45(12): 1464−1471. (in Chinese)
[18] ZHANG Y, FANG Z Z, XIA Y, SUN P, van DEVENER B, FREE M, LEFLER H, ZHENG S L. Hydrogen assisted magnesiothermic reduction of TiO_2 [J]. Chemical Engineering Journal, 2017, 308: 299−310.
[19] MAH A D, KELLEY K K, GELLERT N L, KING E G, O′BRIEN C J. Thermodynamic properties of titanium−oxygen solutions and compounds [M]. Washington DC: Bureau of Mines, 1955.
[20] CHEN G, LISS K D, AUCHTERLONIE G, TANG H, CAO P. Dehydrogenation and sintering of TiH_2: An in situ study [J]. Metallurgical and Materials Transactions A, 2017, 48(6): 2949−2959.
[21] WANG H T, LEFLER M, FANG Z Z, LEI T, FANG S M, ZHANG J M, ZHAO Q. Titanium and titanium alloy via sintering of TiH_2 [J]. Key Engineering Materials, 2010, 436: 157−163.
[22] WANG C M, ZHANG Y A, XIAO S F, CHEN Y G. Sintering densification of titanium hydride powders [J]. Materials and Manufacturing Processes, 2017, 32(5): 517−522.

高钛渣还原的氢化钛合金粉一步烧结制备高强钛合金

董朝望[1,2]，夏 阳[1]，郭学益[1,2]，田庆华[1,2]，刘汉宁[1,2]，刘沛东[1,2]，陈渝冰[1]

1. 中南大学 冶金与环境学院，长沙 410083;
2. 中南大学 资源循环研究院，长沙 410083

摘 要：提出一种直接利用高钛渣制备高强钛合金的方法。先用镁粉还原高钛渣制备氧含量为 1.3%(质量分数)的合金粉末，再将合金粉末在 600 MPa 压力下压制成小圆柱体，最后在氩气下烧结成钛合金产品。对还原粉末进行表征，研究烧结温度对烧结合金的烧后密度、抗压强度、显微组织和硬度的影响。结果表明，随着烧结温度由 900 ℃升高至 1200 ℃，钛合金的密度增加，孔隙率降低，实现较好的烧结致密化(1100 ℃为 98.65%，1200 ℃为 99.41%)，在 1100 ℃时硬度达到 HV 655.7，压缩强度为 1563 MPa。

关键词：高钛渣；还原；钛合金；烧结

(Edited by Xiang-qun LI)